AUGUST 2014 VOL 6 NO 8
www.nature.com/naturechemistry

nature chemistry

MOLECULAR RECOGNITION
Mimicking nature

MAIN GROUP CLUSTERS
Boron buckyballs

SUPER-RESOLUTION MICROSCOPY
Fabricating flashing fluorophores

Topological transplantation in MOFs

nature chemistry

ARTICLES

PUBLISHED ONLINE: 29 JUNE 2014 | DOI: 10.1038/NCHEM.1982

Discovery and introduction of a (3,18)-connected net as an ideal blueprint for the design of metal–organic frameworks

Vincent Guillerm[1], Łukasz J. Weseliński[1], Youssef Belmabkhout[1], Amy J. Cairns[1], Valerio D'Elia[2], Łukasz Wojtas[3], Karim Adil[1] and Mohamed Eddaoudi[1]*

Metal–organic frameworks (MOFs) are a promising class of porous materials because it is possible to mutually control their porous structure, composition and functionality. However, it is still a challenge to predict the network topology of such framework materials prior to their synthesis. Here we use a new rare earth (RE) nonanuclear carboxylate-based cluster as an 18-connected molecular building block to form a gea**-MOF (**gea**-MOF-1) based on a (3,18)-connected net. We then utilized this** gea **net as a blueprint to design and assemble another MOF (**gea**-MOF-2). In** gea**-MOF-2, the 18-connected RE clusters are replaced by metal–organic polyhedra, peripherally functionalized so as to have the same connectivity as the RE clusters. These metal–organic polyhedra act as supermolecular building blocks when they form** gea**-MOF-2. The discovery of a (3,18)-connected MOF followed by deliberate transposition of its topology to a predesigned second MOF with a different chemical system validates the prospective rational design of MOFs.**

The ability to design and construct made-to-order solid-state materials to address ongoing challenges in global energy and environmental sustainability remains elusive. The building-block approach, whereby at the design stage the desired properties and functionality can be introduced in preselected molecular building blocks (MBBs) prior to the assembly process, has emerged as a prominent pathway for the rational construction of functional solid-state materials. The more directional and structural information that can be incorporated into the building block, the higher the degree of predictability and the potential for design[1–4].

Metal–organic frameworks (MOFs)[2,5,6], an emerging class of modular solid-state materials, have attributes (crystallinity, synthesis under mild reaction conditions and an organic/inorganic hybrid composition) that make them amenable to construction using the MBB approach[1]. Nevertheless, several key prerequisites have to be fulfilled for the design and directed assembly of MOFs with specific, pre-selected network topologies. Generally, the blueprint net should be a minimal-edge transitive net[7] (a net with only one or two kinds of edge) that is exclusive for the assembly of its corresponding basic building units[8,9]. Additionally, the points of extension of the requisite building blocks (the points at which the building blocks are joined together to form a net) should match the vertices of the corresponding vertex figure in the targeted net. Typically, for a given net, an *n*-connected node is replaced by a related polygon or polyhedron with *n* vertices (vertex figure); such a process is referred to as a net augmentation and results in an augmented net (**net**-a). A resultant vertex figure dictates the requisite *n* connectivity (*n* points of extension), structural and geometrical information to be targeted and expressed in a chemical building block entity prior to the directed assembly process into a net. Practically, highly connected nets with at least one *n*-connected node, where $n \geq 12$, are suitable targets in crystal chemistry, as they limit the number of outcome nets for the assembly of their associated highly connected building blocks[10]. Potentially, such building blocks can be accessed chemically through either MBBs or supermolecular building blocks (SBBs). Highly connected metal clusters can be used as MBBs[8,9,11–17], and more-elaborate metal–organic polyhedra (MOPs), based on the assembly of relatively simple and readily accessible three- or four-connected MBBs, can be employed as SBBs. Our group is actively pursuing both of the aforementioned pathways, namely (1) exploring various metal and functional ligand coordination chemistries with the aim of discovering new modular highly connected polynuclear metal clusters[14] and (2) investigating particular nets that are amenable to the synthesis and design of MOFs through the SBB approach[9,18,19].

In this report, we describe the isolation of highly connected polynuclear clusters and their use as MBBs in MOF synthesis. We also demonstrate the power of the SBB approach in facilitating the design and deliberate construction of MOF structures. We present the discovery and formation, *in situ*, of a novel rare earth (RE) nonanuclear carboxylate cluster $[RE_9(\mu_3\text{-}OH)_8(\mu_2\text{-}OH)_3(O_2C\text{–})_{18}]$, (RE = Y, Tb, Er, Eu). This serves as an 18-connected MBB for the assembly of a (3,18)-connected MOF with an unusual **gea** topology, **gea**-MOF-1. Using the SBB approach, we then demonstrate that replacing the relatively simple and dense 18-connected inorganic MBBs by more complex and more open Cu-based MOPs, acting as 18-connected SBBs, is a viable route to MOF design. Using the newly discovered (3,18)-connected net as a blueprint and combining it with the 18-connected SBBs, we also report the deliberate construction of a related **gea**-MOF, **gea**-MOF-2.

Results and discussion

Discovery of an 18-connected RE nonanuclear cluster and a (3,18)-connected net. MOFs constructed from RE metal ions and/or clusters are of prime interest for building multifunctional

[1]Functional Materials Design, Discovery and Development Research Group (FMD[3]), Advanced Membranes and Porous Materials Center (AMPM), Division of Physical Sciences and Engineering, King Abdullah University of Science and Technology (KAUST), Thuwal 23955-6900, Kingdom of Saudi Arabia, [2]Kaust Catalysis Center (KCC), King Abdullah University of Science and Technology (KAUST), Thuwal 23955-6900, Kingdom of Saudi Arabia, [3]Department of Chemistry, University of South Florida, 4202 East Fowler Ave., Tampa, Florida 33620, USA. *e-mail: mohamed.eddaoudi@kaust.edu.sa

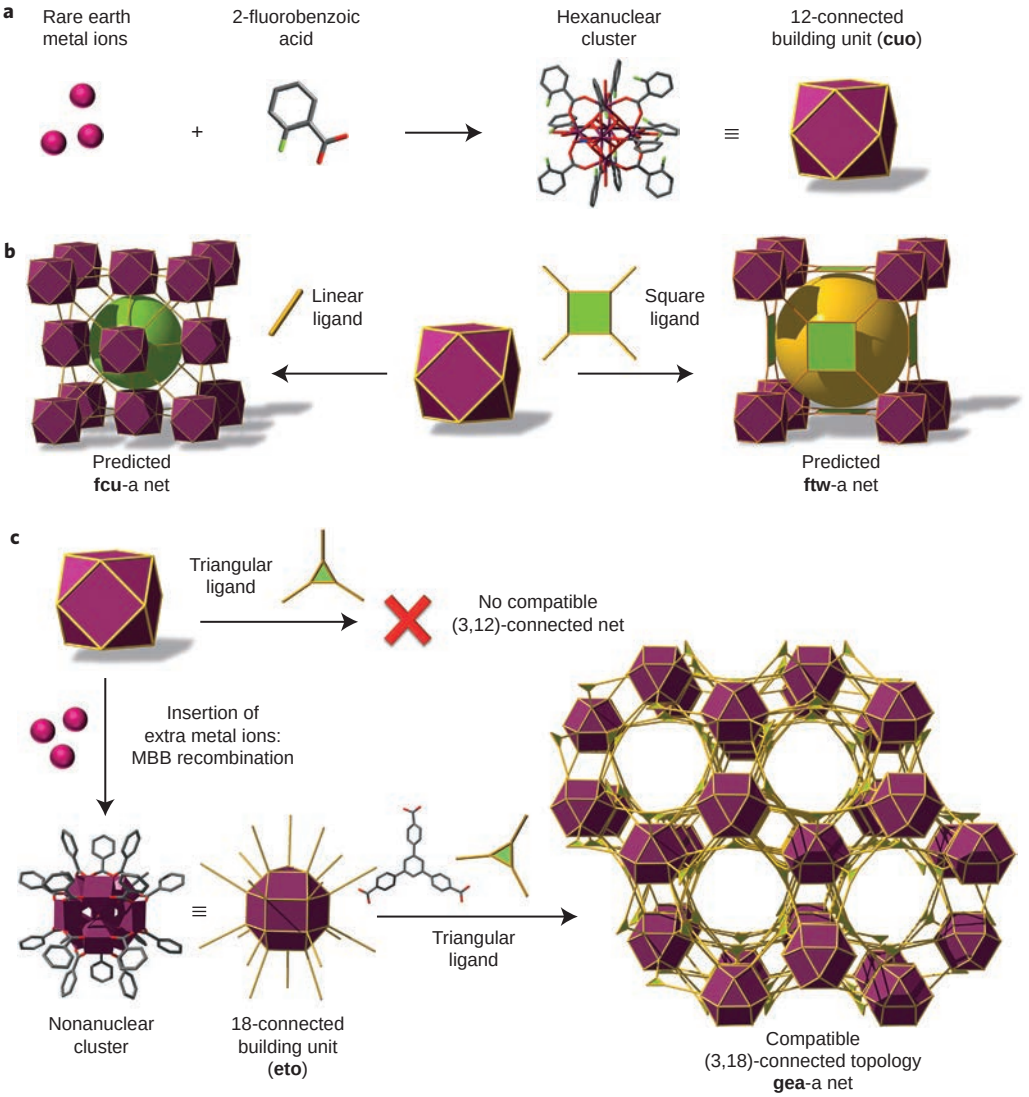

Figure 1 | Topological exploration that led to the discovery of gea**-MOF-1. a**, A combination of RE metal ions and 2 fluorobenzoic acid enables the assembly of a hexanuclear RE cluster. The carbon atoms of the carboxylate ligands (that is, the points of extension) coincide with the 12 vertices of a **cuo**, which enables the hexanuclear cluster to act as a 12-connected molecular building block for MOF formation. **b**, Linking of 12-connected MBBs with either linear (two-connected) or square (four-connected) MBBs results in the formation of a **fcu** net or a **ftw** net, respectively. **c**, The 12-connected MBBs do not form structures when combined with triangular (3-connected) MBBs; however, the insertion of three extra RE ions into the hexanuclear cluster affords the evolution of a nonanuclear cluster coordinated by 18 carboxylate ligands. In this cluster, the points of extension coincide with the 18 vertices of an **eto** polyhedron. It therefore acts as an 18-connected MBB and, in combination with a triangular MBB, affords the assembly of a (3,18)-connected net, the **gea** net. In the skeletal molecular structures in **a** and **c**, RE, C, O and F are represented by purple, grey, red and light green, respectively, and H atoms are omitted for clarity. For clarity, **fcu**, **ftw** and **gea** topologies are represented as augmented nets.

materials as a result of their intrinsic properties (for example, catalysis and luminescence). However, their deliberate construction remains an ongoing challenge because the RE hard-sphere behaviour limits the ability to control the directionality of coordinated ligands, and therefore it is difficult to control the resulting MOF structural outcomes[20–26].

Recently, our discovery of a RE-based face-centred cubic (**fcu**) MOF platform allowed fine-tuning of the appropriate reaction conditions for the consistent *in situ* formation of the hexanuclear RE cluster $[RE_6(\mu_3\text{-}OH)_8(O_2C\text{–})_{12-x}(N_4C\text{–})_x$, $x = 0, 8]$, a 12-connected inorganic MBB ideal for MOF crystal chemistry[14]. These reaction conditions, in the presence of 2-fluorobenzoic acid (2-FBA), were employed in the absence of bridging or terminal ligands to form the corresponding discrete hexanuclear cluster. We were able to grow and isolate single crystals via prolonged slow evaporation of the reaction mixture. They were formulated by single-crystal diffraction (SCD) data as $[RE_6(\mu_3\text{-}OH)_8(O_2C\text{–}C_6H_4F)_{11}(DMF)(NO_3^-)(H_2O)_6]$ (RE = Tb, DMF = dimethylformamide). It is proposed that the presence of 2-FBA could play a major role in repelling water molecules and might explain the formation of discrete multinuclear clusters rather than the infinite RE chains commonly observed in RE-MOFs (Fig. 1a)[20,21,24–26].

Our analysis of the Reticular Chemistry Structure Resource (RCSR) database[10] showed that such a 12-connected MBB (cuboctahedron (**cuo**) building units) can potentially be linked via four-connected MBBs (square building units) or directly bridged (with two-connected linear ligands) to afford MOFs with **ftw**[16] or **fcu**[11,13–15] topologies, respectively (Fig. 1b). However, to the best of our knowledge, there is no reported topology possible for the assembly of the present 12-connected MBB (points of extension matching the vertices of the **cuo**) with triangles. In the predicted (3,12)-connected **ttt** net, the corresponding compatible 12-connected building block (truncated tetrahedron is the

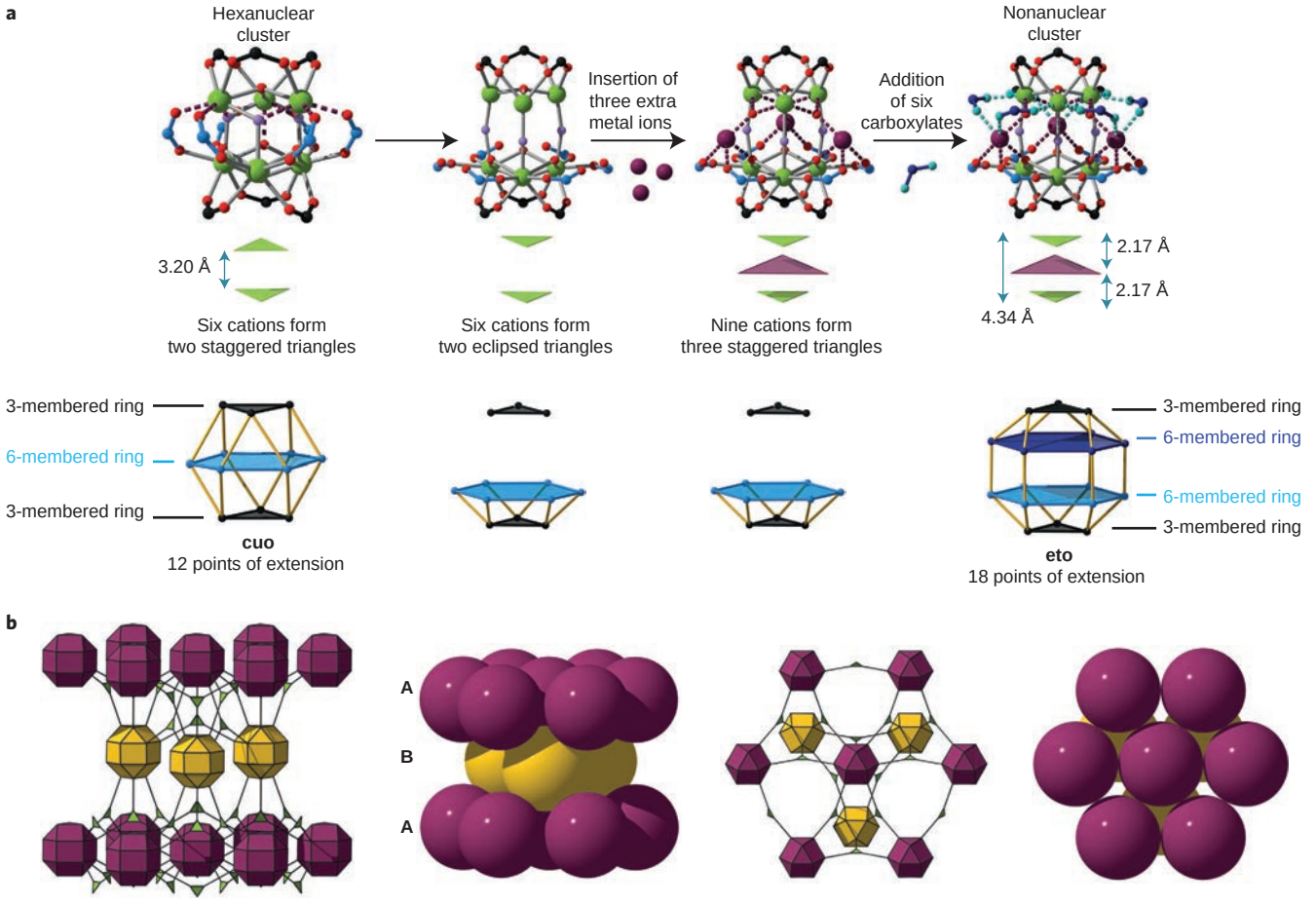

Figure 2 | Cluster rearrangement and packing in gea**-MOF-1. a**, A proposed path that shows the evolution from the hexanuclear to the nonanuclear cluster. The upper part shows the hexanuclear cluster on its evolution into a nonanuclear cluster. The green triangles directly underneath represent the spatial arrangement of the RE atoms in the cluster and show the 30° rotation and the addition of three RE metal ions. The lower part demonstrates the effect of cluster evolution on the MBB points of extension, which increase from 12 (**cuo**) to 18 (**eto**). RE atoms from the hexanuclear cluster are in light green, and the additional RE atoms needed to form the nonanuclear cluster are in purple; C atoms from the carboxylates are in black for the top and bottom of the cluster (3-membered rings), and blue for the middle (6-membered rings). **b**, Views of the hexagonal close packing of the MBBs of **gea**-MOF-1. A and B layers from the hexagonal packing are represented in purple and yellow, respectively.

vertex figure of the 12-connected node) has a very different shape to that of a **cuo**. Such a mismatch offers great opportunity to discover plausible highly connected RE polynuclear clusters and their respective assembly into MOFs with potentially novel topologies.

The combination of 1,3,5-benzene(tris)benzoate (BTB) and RE without 2-FBA gives MOFs with extended building units (chains) and modest porosity (Supplementary Fig. 10)[21,24–26], but the ability to form consistently the 12-connected RE hexanuclear cluster combined with its apparent non-compatibility with triangular ligands has propelled us to use BTB as a potential vehicle to derive a new highly connected RE cluster for the construction of MOFs (Fig. 1c).

Reactions between H_3BTB and $Y(NO_3)_3{\cdot}6H_2O$ in the presence of 2-FBA in an *N*,*N*′-DMF/water solution yielded hexagonal rod-shaped crystals (Supplementary Fig. 9), formulated by SCD and elemental analysis as $(DMA^+)_2[Y_9(\mu_3\text{-}OH)_8(\mu_2\text{-}OH)_3((O_2C\text{–}C_6H_4)_3C_6H_3)_6]_n{\cdot}(solv)_x$ (DMA^+ = dimethylammonium cations, solv = solvent). Structural and topological analysis of the resulting crystal structure reveals the formation of a (3,18)-connected MOF based on a polynuclear RE cluster $[Y_9(\mu_3\text{-}OH)_8(\mu_2\text{-}OH)_3(O_2C\text{–})_{18}]$, a distinctive 18-connected MBB linked to the triangular BTB to form a MOF with a (3,18)-connected net and **gea** topology (Fig. 1c). The discovery of the **gea** topology led us to explore the possible occurrence of other related (3,18)-connected nets, and we were able to uncover a second (3,18)-connected net of **gez** topology, where the 18-connected node has a vertex figure that matches the elongated triangular gyrobicupola (**etg**) (Johnson solid (J_{36}); see the Supplementary Information).

Analysis of the $[Y_9(\mu_3\text{-}OH)_8(\mu_2\text{-}OH)_3(O_2C\text{–})_{18}]$ cluster revealed its close relation to the $[Y_6(\mu_3\text{-}OH)_8(O_2C\text{–})_{12}]$ cluster, but with three additional metal ions incorporated (Fig. 2a and Supplementary Fig. 18). Also isolated from 2-FBA-assisted reactions of BTB with nitrate-based salts of RE, this RE-MBB, $[RE_9(\mu_3\text{-}OH)_8(\mu_2\text{-}OH)_3(O_2C\text{–})_{18}]$ (RE = Y, Tb, Er, Eu (Supplementary Fig. 12)), is built from nine metal ions arranged in a tricapped trigonal prism (**tct** (J_{51})). Six of the yttrium ions are coordinated to eight oxygen atoms (that is, four from the carboxylates, three μ_3-OHs and one μ_2-OH) with the coordination mode of the remaining three sites reduced to six (that is, four O from the carboxylates and two μ_2-OHs). The overall cluster is anionic $[Y_9(\mu_3\text{-}OH)_8(\mu_2\text{-}OH)_3(O_2C\text{–})_{18}]^{2-}$, and the resultant framework overall charge is probably balanced by DMA^+ generated *in situ* from the decomposition of DMF solvent molecules. The yttrium cluster is capped by 18 carboxylates from 18 different BTB ligands (Fig. 1c) to give an 18-connected MBB, elongated triangular orthobicupola (**eto**) building unit with 18 vertices (J_{35}, Fig. 1c). Inspection of **gea**-MOF-1 also reveals hexagonal close packing of the nonanuclear cluster MBBs and thus can be simplified as pillared hexagonal (**hxl**) layers (Fig. 2b and Supplementary Figs 20–22).

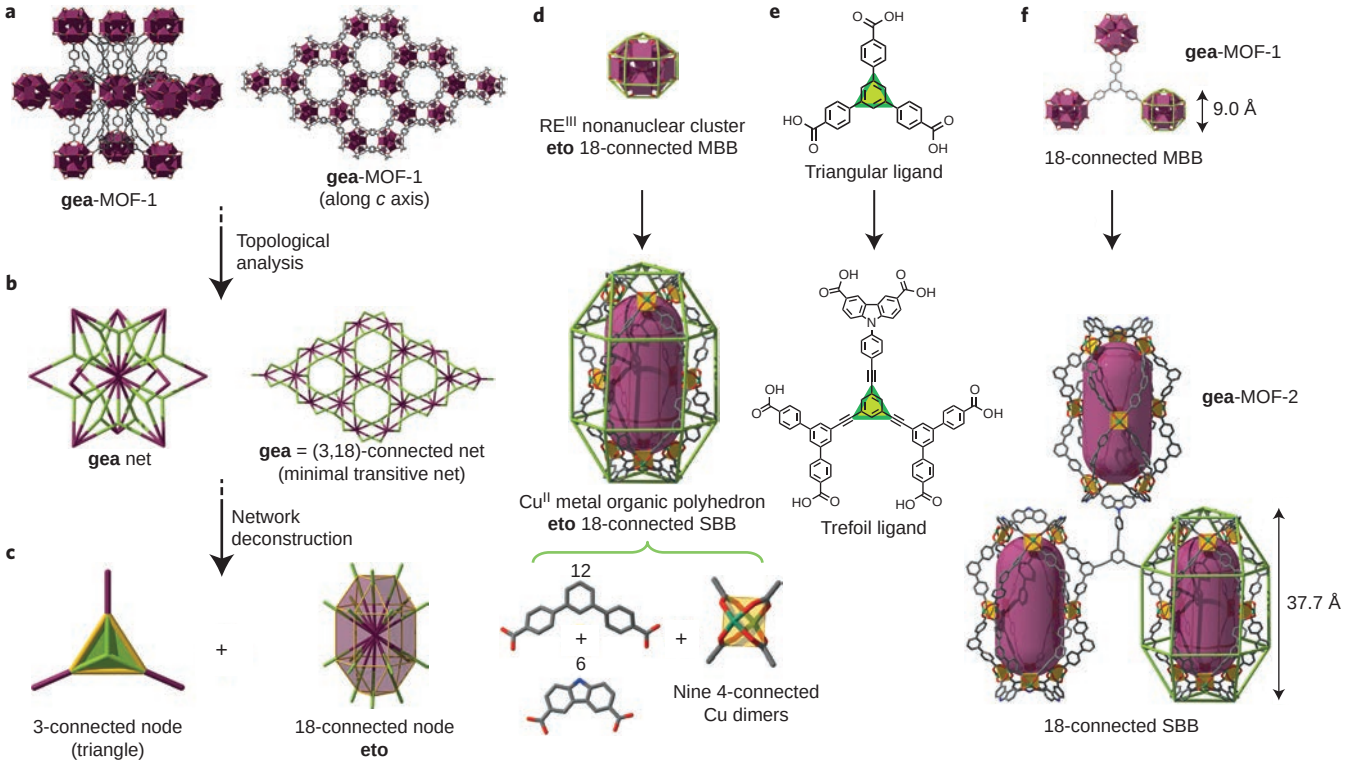

Figure 3 | SBB approach to design expanded gea**-MOF-2. a**, Structural representations of **gea**-MOF-1. **b**, Topological analysis of **gea**-MOF-1 reveals the underlying (3,18)-connected **gea** net. **c**, The augmented 18-connected and 3-connected nodes that make up the underlying **gea** net have vertex figures of an **eto** and a triangle, respectively, and these vertex figures can be taken as general building blocks in the construction of other MOFs with **gea** topology. **d**, Using these vertex figures, the SBB approach allows the substitution of the 18-connected **eto** cluster with an 18-connected **eto** MOP. This MOP is itself constructed from nine square Cu dimers and 18 organic ligands: 12 bent dicarboxylic acids with a 120° angle between coordination sites and six dicarboxylic acids with a 90° angle. **e**, Substitution of the three-connected triangular ligand in **gea**-MOF-1 with a designed $\mathbf{H_6L}$ ligand. $\mathbf{H_6L}$ was designed to be compatible with the (3,18)-connected **gea** net by possessing the same triangular core and the appropriate ratio of dicarboxylic acid moieties. **f**, The 18-connected building blocks are linked by a triangular core in both **gea**-MOF-1 and **gea**-MOF-2, but the sizes of the building blocks are different in each MOF.

Alternatively, the topology of the **gea**-MOF-1 (3,18)-connected net, minimal transitivity [2244] (Supplementary Fig. 19), can be viewed as a more-open variant of the ubiquitous (3,24)-connected **rht** net pioneered by Eddaoudi and co-workers[9]. The rhombicub-octahedron (24 vertices) from **rht** is substituted by the **eto** in **gea**-MOF-1 with only 18 vertices. The reduced number of points of extension leads to the occurrence of channels within the structure, not present in **rht**-MOFs (Supplementary Figs 20–24).

Rational design of MOFs using the (3,18)-connected net and the SBB approach. Highly connected MBBs, such as the nonanuclear RE cluster described above, have potential for the design of MOFs as their possible assembly into extended structures offers a limited number of outcome nets. One idea to aid the rational design of new MOFs would be the transposition of the **gea** topology into a second MOF, using the SBB approach[8,9,18,27]. The SBB approach employs a given MOP (in this case, in place of the RE cluster) as a highly connected building block. Indeed, the newly disclosed highly connected binodal **gea** net (Fig. 3a–c), which encompasses only two kinds of edge and is not self-dual, is an ideal blueprint for MOF crystal chemistry. The 18-connected dense RE cluster from **gea**-MOF-1 can be substituted elegantly with a relatively open MOP, itself assembled from square MBBs (Fig. 3d). The primary requirement to translate the augmented **gea** (**gea**-a) blueprint net into practice for MOF chemistry is to construct a MOP that acts as an 18-connected SBB in which its points of extension coincide with the geometrical building unit that corresponds to the augmentation of the 18-connected vertex (that is, vertex figure) of the given **gea** net. Accordingly, our survey of the Cambridge Structural Database and open literature revealed the existence of such an **eto** MOP based on nine copper paddlewheels $[Cu_2(O_2CR)_4]$ bridged by 12 4,4′-(pyridine-2,6-diyl) dibenzoic acids with a 120° angle and six carbazole-3,6-dicarboxylic acids with a 90° angle[28]. In this MOP, the bent

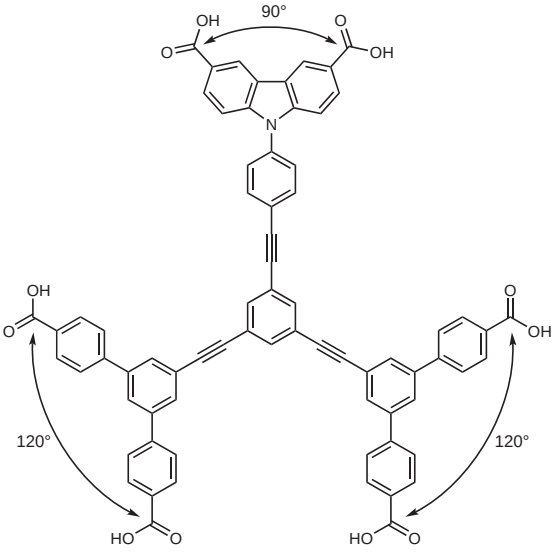

$\mathbf{H_6L}$
Ligand for **gea**-MOF-2

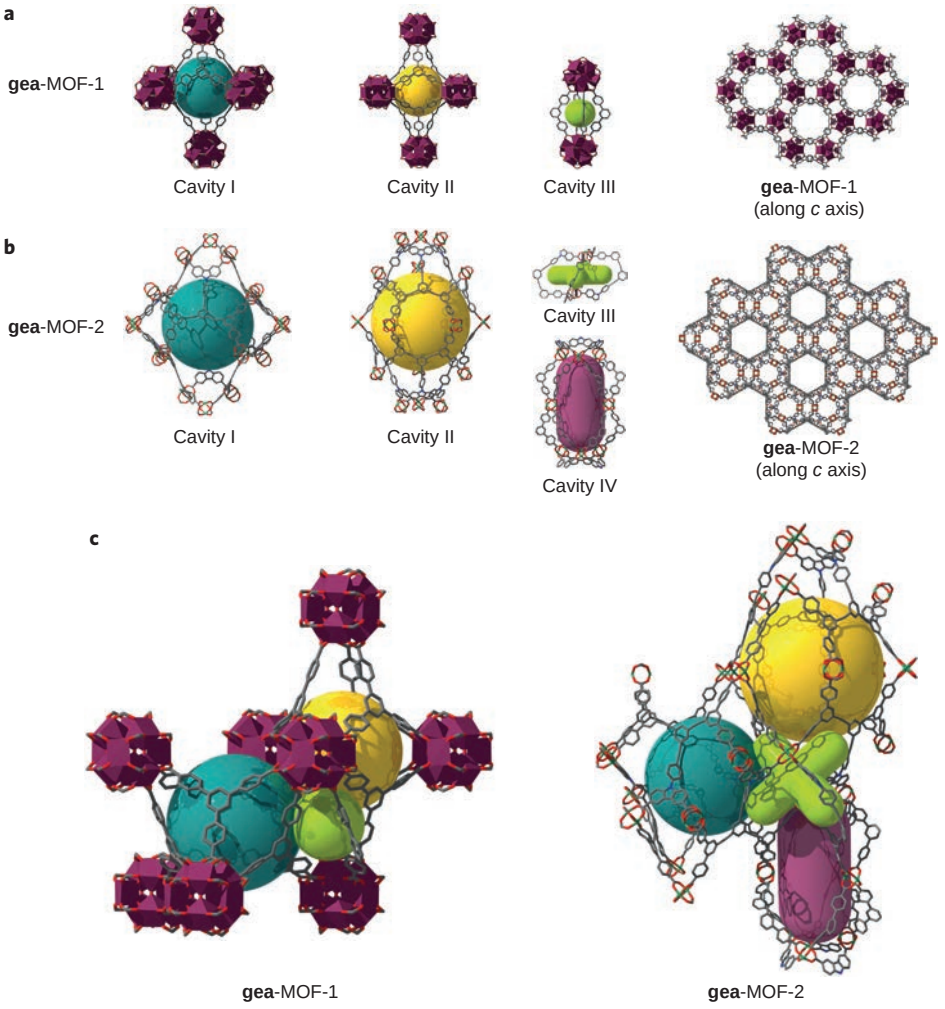

Figure 4 | Relationship between gea**-MOF-1 and** gea**-MOF-2. a**, Open spaces and general view of **gea**-MOF-1 reveal three types of cavity. **b**, Open spaces and general view of **gea**-MOF-2 showing that **gea**-MOF-1 and **gea**-MOF-2 are structurally related, but that **gea**-MOF-2 has an extra cavity relative to **gea**-MOF-1. **c**, The packing of the cavities in **gea**-MOF-1 and **gea**-MOF-2 are similar, but the nonanuclear RE clusters in **gea**-MOF-1 are replaced by cavity IV in **gea**-MOF-2. RE, Cu, C, N and O are represented in purple, green, grey, blue and red, respectively. For clarity, H atoms are omitted and the relative scales of **gea**-MOF-1 and **gea**-MOF-2 are not the same.

position of each of these 18 ligands lies perfectly on the vertices of the desired **eto** SBB (Fig. 3d). Further geometrical analysis of the **gea**-a net revealed that transposition of such an SBB into the anticipated **gea**-MOF platform required the employment of a trefoil-like ligand encompassing two branches that contain 120° angle dicarboxylic acid extremities and a third branch with a 90° angle dicarboxylic acid extremity (Fig. 3e,f).

Consequently, we designed such a trefoil-like hexacarboxylate ligand for both the formation of the targeted MOP and their subsequent linking in a triangular fashion, as dictated by the connectivity in the central core of the ligand (Fig. 3f). We thus embarked on the multistep ligand synthesis of 5′,5‴′-((5-((4-(3,6-dicarboxy-9H-carbazol-9-yl)phenyl)ethynyl)-1,3-phenylene)bis(ethyne-2,1-diyl))bis((1,1′:3′,1″-terphenyl]-4,4″-dicarboxylic acid), referred to as $\mathbf{H_6L}$ (Supplementary Figs 1–8).

As envisioned, reaction of $\mathbf{H_6L}$ with copper cations yielded a **gea**-MOF of very low density (calculated density ≈ 0.29 g cm^{-3}, free volume $\approx 85\%$ for the solvent-free structure), **gea**-MOF-2, which exhibited the anticipated (3,18)-connected topology (considering the 18-connected MOP as a node for the topological analysis, Supplementary Fig. 28). This demonstrates that edge transitive nets are not the only ideal suitable targets in crystal chemistry, but that highly connected binodal nets with two kinds of edge (and minimal transitivity, that is minimum numbers of kinds of vertices and edges) are also appropriate targets when sufficient coded directional and geometrical information can be included directly in the SBB.

This **gea**-MOF-2, formulated $[(Cu_3(L)(H_2O)_3]_n\cdot(solv)_x$ by SCD, crystallizes in a hexagonal system, the same as **gea**-MOF-1 but with a larger cell volume (88,962(5) Å^3 versus 14,165.6(12) Å^3), theoretical pore volume (2.76 cm^3 g^{-1} versus 0.71 cm^3 g^{-1}), free volume (85.6% versus 61.7%) and much lower calculated density (0.29 g cm^{-3} versus 0.84 g cm^{-3}). **gea**-MOF-1 exhibits three distinct cages (van der Waals (vdW) distances: cavity I, 22.4 Å × 22.4 Å; cavity II, 24.8 Å × 14.6 Å; cavity III, 11.2 Å × 5.6 Å), cavity I being seen as a channel (aperture, vdW distances 12.8 Å × 9.4 Å) (Fig. 4a and Supplementary Figs 25–27), and **gea**-MOF-2 exhibits a related pore system (vdW distances: cavity I, 41.7 Å × 34.2 Å; cavity II, 44.5 Å × 33.6 Å; cavity III, 21.2 Å × 6.5 Å) (Fig. 4b,c and Supplementary Fig. 29), but also contains an additional fourth cavity (cavity IV, **eto** $[3^8.4^{12}]$, vdW distances 26.6 Å × 15.6 Å) because of the substitution of the relatively dense inorganic cluster by an open MOP. Further geometrical studies showed that the structure is expandable through five independent parameters (Supplementary Fig. 31), which allows a higher degree of tunability than that in **rht**-MOFs, for which only two independent expansion parameters have been reported thus far.

From a purely topological point of view, this structure should certainly be described as the unprecedented and complex **gwe** topology: (3,3,3,4,4)-connected net, transitivity [5575], and it can also be regarded in other distinct ways (see Supplementary Figs 29 and 30). Nevertheless, such a pentanodal net is far too convoluted and illustrates the difficulty in using the **gwe** net basic building units, namely squares and triangles, as a rational means to target MOFs based on this topology. It also shows the effectiveness of the SBB approach based on more elaborate building units (SBB, a MOP constructed from nine square copper paddlewheels $[Cu_2(O_2CR)_4]$ bridged by 18 ligands) in embedding hierarchical information and thus coding for the rational design of a **gea**-related MOF, **gea**-MOF-2. Evidently, the SBB approach offers potential for systematically substituting dense clusters by relatively open MOPs (Fig. 3d,f) to access additional functionalized spaces within more simple and already known nets (**fcu**, **pcu**, etc.) by careful choice of SBBs.

In fact, as the complex pentanodal (five distinct vertices) **gwe** net is a descendent net of the **gea** net, it would have been *in fine* possible to design MOFs with **gwe** topology using the SBB approach, by first recognizing its relationship to the **gea** net and then employing gea-coded building units (namely the 18-connected **eto** polyhedron and a triangle) if the **gea** and **gwe** nets were enumerated beforehand. Broadly, we anticipate that certain complex polynodal nets can be partially deconstructed into their embedded polyhedra or layers; that is, keeping some of their basic building units grouped into elaborated building units coding for the net (**net**-coded building units). In this way, this report opens the door to a new way of thinking about designing solid-state materials by looking into extended solids from an alternative perspective.

Sorption and catalytic properties. In light of the interesting chemical and structural properties of **gea**-MOF-1, we explored its use in a number of applications such as gas storage, CO_2 capture, hydrocarbon separation (Supplementary Figs 37–43) and CO_2 conversion[29,30].

Investigation of Ar adsorption at 87 K showed that **gea**-MOF-1 exhibits a fully reversible Type-I isotherm (Supplementary Fig. 36), representative of porous materials with permanent microporosity. The apparent Brunauer–Emmett–Teller (BET) and Langmuir surface areas and the pore volume were estimated to be 1,490 $m^2 g^{-1}$, 1,600 $m^2 g^{-1}$ and 0.58 $cm^3 g^{-1}$, respectively, which are in good agreement with the derived theoretical values[31], and significantly higher than those reported for other RE-BTB MOFs ($280 < S_{BET} < 930\ m^2 g^{-1}$) [21,25]. Interestingly, the **gea**-MOF-1 maintains its optimal porosity on heating up to 360 °C under vacuum (Supplementary Fig. 35), which so far has rarely been reported for MOFs[24,32]. This valuable finding is also in agreement with the data from the variable-temperature powder X-ray diffraction studies (VT-PXRD, Supplementary Fig. 13) and thermogravimetric analysis (TGA, Supplementary Fig. 14).

Examination of excess and absolute CH_4 gravimetric (mmol g^{-1}) and volumetric (cm^3 (STP) cm^{-3}) uptakes at intermediate and high pressures showed that **gea**-MOF-1 adsorbs 40, 140 and 162 cm^3 (STP) cm^{-3} of CH_4 at 5, 35 and 50 bar, respectively (Supplementary Fig. 40). The resulting CH_4 working storage capacities, assuming 35 bar (following the US Department of Energy standard) and 50 bar as the highest adsorption pressure and 5 bar as the lowest desorption pressure (following the requirement of the engine methane injection pressure)[33] (Supplementary Tables 4 and 5), are about 100 and 122 cm^3 (STP) cm^{-3}, respectively. For the highest pressure limit of 35 bar, this volumetric working capacity, calculated assuming the density of **gea**-MOF-1 is constant and equivalent to the theoretical density, is similar to the corresponding working capacity reported for UiO-67(Zr)[34], largely higher than UTSA-20 (about 80 cm^3 (STP) cm^{-3})[35], but still lower than the working CH_4 storage capacity calculated for HKUST-1[36] and NU-125[33] (about 150 and 120 cm^3 (STP) cm^{-3}). Assuming the highest pressure limit at 50 bar, the volumetric working capacities for NU-125 and HKUST-1 were found to be the highest (about 170 and 175 cm^3 STP cm^{-3}, respectively) (Supplementary Table 5).

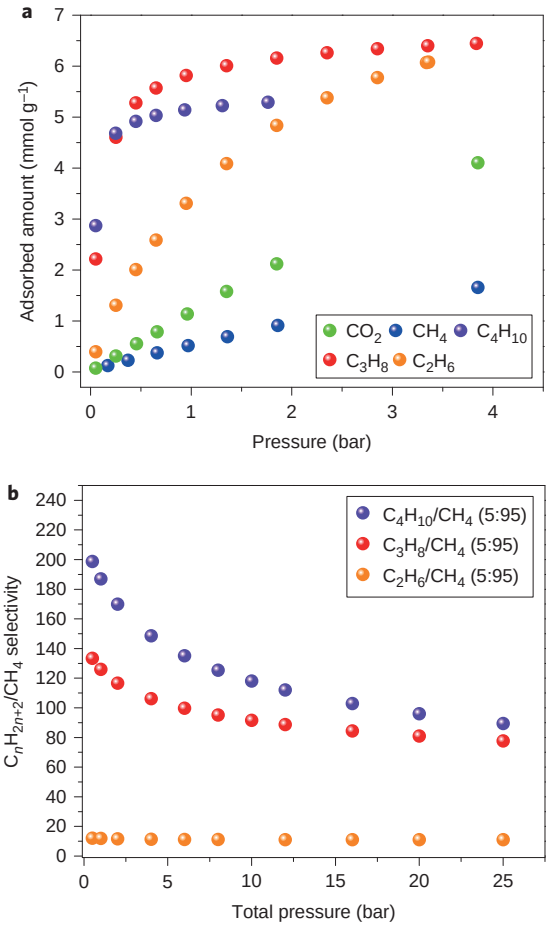

Figure 5 | gea**-MOF-1 shows great potential for hydrocarbon separation.** **a**, CH_4, CO_2, C_2H_6, C_3H_8 and n-C_4H_{10} single gas adsorption isotherms at 298 K. Based on the gradient of the isotherms at low pressure, the affinity of these molecules for **gea**-MOF-1 follows the sequence n-$C_4H_{10} > C_3H_8 \gg C_2H_6 > CO_2 > CH_4$. **b**, Predicted selectivities in the adsorption of gas mixtures with molar ratios of C_2H_6/CH_4 (5:95), C_3H_8/CH_4 (5:95) and n-C_4H_{10}/CH_4 (5:95) using IAST calculations. Selectivity is defined by the ratio of C_nH_{2n+2} to CH_4 in the phase adsorbed to **gea**-MOF-1, versus the initial gas-phase composition (5:95). These predict very high selectivity for n-C_4H_{10} and C_3H_8 over CH_4 and high selectivity for C_2H_6 over CH_4 for **gea**-MOF-1. The different selectivity behaviour of **gea**-MOF-1 towards C_nH_{2n+2} is mainly governed by the difference in the polarizabilities of the alkane species.

To investigate the adsorption of larger and highly polarizable probe molecules, we studied the adsorptions on **gea**-MOF-1 of C_2H_6, C_3H_8 and n-C_4H_{10} (C_nH_{2n+2}) up to 4 bar and compared these to CO_2 and CH_4 adsorption capabilities, to assess **gea**-MOF-1's potential use in natural gas upgrading (Fig. 5a). It is significant that, despite the importance of hydrocarbon separation (for example, the purification of CH_4 from condensable hydrocarbons such as C_2H_6, C_3H_8 and n-C_4H_{10}), only a few studies have focused on the selective adsorption of condensable hydrocarbons[26,37–40].

Interestingly, the C_nH_{2n+2} adsorption isotherms were much steeper at low pressure than those for CH_4 and CO_2, indicative of the high affinity of **gea**-MOF-1 to C_nH_{2n+2}. Examination of single adsorption data using ideal adsorption solution theory (IAST) confirmed the high selectivity of C_nH_{2n+2}/CH_4, particularly for gas pair systems such as C_3H_8/CH_4 and n-C_4H_{10}/CH_4 (Fig. 5b). Therefore, **gea**-MOF-1 can be employed as a C_3H_8/CH_4 and n-C_4H_{10}/CH_4

Table 1 | Catalytic activity of gea-MOF-1: synthesis of cyclic carbonates from CO_2 and epoxides catalysed by gea-MOF-1.

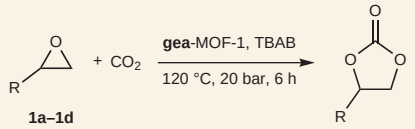

1a–1d **2a–2d**

R = Me (**a**), Et (**b**), Ph (**c**), CH_2Cl (**d**)

Entry	R	Catalyst	Conversion (%)*	TON†	TOF (h^{-1})‡
1§	Me	YCl_3, TBAB	80	800	1,067
2‖	Me	YCl_3, TBAB	75	75	19
3	Me	TBAB	16	-	-
4¶	Me	Y_2O_3, TBAB	29	97	16
5	Me	**gea**-MOF-1	6	40	7
6	Me	**gea**-MOF-1, TBAB	88	587	98
7#	Me	**gea**-MOF-1, TBAB	86	573	96
8#	Me	**gea**-MOF-1, TBAB	80	533	89
9#	Me	**gea**-MOF-1, TBAB	77	513	86
10	Et	**gea**-MOF-1, TBAB	94	627	105
11	Ph	**gea**-MOF-1, TBAB	85	567	94
12	CH_2Cl	**gea**-MOF-1, TBAB	89	593	99

Unless otherwise noted all reactions were carried out by using epoxides **1a–1d** (100 mmol), **gea**-MOF-1 (60 mg, corresponding to 0.15 mmol yttrium), TBAB (0.15 mmol) at 120 °C, 20 bar for six hours. *Conversion evaluated from the ^{1}H NMR spectra by integration of epoxide versus cyclic carbonate peaks. †Turnover number (product (mmol)/yttrium (mmol)). ‡Turnover frequency. §**1a** (100 mmol), YCl_3 (0.1 mmol), TBAB (0.1 mmol) at 100 °C, 10 bar for 45 minutes. ‖**1a** (100 mmol), YCl_3 (1 mmol), TBAB (2 mmol) at 25 °C, 1 bar CO_2 for four hours. ¶**1a** (100 mmol), Y_2O_3 (0.15 mmol), TBAB (0.15 mmol). #With recycled **gea**-MOF-1 from the previous entry.

separation agent for natural gas upgrading because of its high affinity for C_3H_8 and n-C_4H_{10} versus CH_4 and CO_2.

In view of the high accessibility of the extended network of exposed metal centres and of its remarkable thermal stability, we then explored the relevance of **gea**-MOF-1 for heterogeneous catalysis in the cycloaddition of CO_2 and epoxides. CO_2 is regarded as an inexpensive C-1 source for the preparation of bulk chemicals[41,42] and cyclic organic carbonates, a feedstock for a wide range of applications in industry[43–45]. Recently, thermally stable porous materials have proved to be efficient heterogeneous catalysts for the coupling of CO_2 and epoxides[46]. As no yttrium-based catalysts have been reported for this reaction so far, we initially tested simple YCl_3 as a homogeneous catalyst for the cycloaddition of CO_2 and propylene oxide. Interestingly, YCl_3/TBAB (TBAB = tetrabutylammonium bromide) formed a powerful catalytic system for the conversion of CO_2; high catalytic activity was observed under mild temperature and pressure (100 °C, 10 bar), and under ambient conditions the catalytic performance was comparable to that of the recently reported $NbCl_5$/TBAB pair (Table 1, entries 1 and 2)[46].

This result underlines the high potential of yttrium-based catalytic systems towards CO_2 conversion. Therefore, we tested **gea**-MOF-1 (as a heterogeneous catalyst) under similar pressure and temperature conditions to those used for the YCl_3 test (homogeneous catalyst). As seen from Table 1, the tests on **gea**-MOF-1 proved that it can serve as an excellent recoverable catalyst for the solvent-free synthesis of carbonates **2a–2d** under mild conditions in the presence of co-catalytic amounts of TBAB (Table 1, entries 6–12, Supplementary Table 6 and Supplementary Fig. 44). The material could be reused without showing any significant drop in catalytic performance (Table 1, entries 6–9). Readily available Y_2O_3 was also tested as a heterogeneous catalyst for this reaction under similar conditions and, as expected, the catalytic results were significantly lower. The superior catalytic activity observed for **gea**-MOF-1 can be attributed to the higher accessibility of the Lewis acid yttrium sites, which is deemed necessary for epoxide activation as a first reaction step.

Conclusions

We report here our latest progress in investigating highly coordinated polynuclear inorganic clusters and highly connected nets as targets in crystal chemistry. We synthesized and characterized a RE-MOF, formed from a nonanuclear RE cluster acting as an 18-connected inorganic MBB. This previously unknown cluster, seemingly accessible only through our modulated approach using fluorinated benzoic acid, has led to the discovery of a non-self-dual (3,18)-connected **gea** net. It is hoped that this approach will permit, in the near future, re-exploration of other previously studied RE-based systems. Encouragingly, the isolated **gea**-MOF-1 exhibits potential for CH_4-storage applications as well as for butane/methane and propane/methane separations. Interestingly, yttrium-based **gea**-MOF-1 also shows catalytic activity in the coupling of CO_2 and epoxides.

This work on **gea**-MOFs is, to the best of our knowledge, the only example in which a previously unknown topology has been discovered in a specific system (that is RE^{III}–tricarboxylate) and successfully transposed into a drastically different chemical system (Cu^{II}–hexacarboxylate) by replacing dense inorganic clusters with relatively open MOPs. We clearly demonstrate and corroborate the power of the SBB approach for the deliberate construction of **gea**-MOFs as an exemplary platform for ready-made functional materials.

Moreover, the partial deconstruction of complex nets into their embedded polyhedra opens the door to new ways of thinking about designing solid-state materials, and suggests that material designers should explore the myriad of design options offered by the SBB approach.

Methods

Preparation of $[Tb_6(\mu_3\text{-}OH)_8(O_2C\text{–}C_6H_4F)_{11}(DMF)(NO_3^-)(H_2O)_6]$, a Tb hexanuclear cluster. A solution of $Tb(NO_3)_3{\cdot}5H_2O$ (21.8 mg, 0.05 mmol), 2-FBA (56.4 mg, 0.4 mmol), DMF (2 ml) and H_2O (0.5 ml) was prepared in a 20 ml scintillation vial and subsequently heated to 105 °C for 36 hours in a preheated oven. The solution was then left to evaporate slowly at room temperature under air in a ventilated fume hood. After approximately two months, a few octahedral crystals were harvested (Supplementary Fig. 32 and Supplementary Table 1).

Preparation of $(DMA^+)_2[Y_9(\mu_3\text{-}OH)_8(\mu_2\text{-}OH)_3((O_2C\text{–}C_6H_4)_3C_6H_3)_6]_n{\cdot}(solv)_x$, gea-MOF-1. A solution of $Y(NO_3)_3{\cdot}6H_2O$ (8.6 mg, 0.0225 mmol), H_3BTB (6.6 mg, 0.015 mmol), 2-FBA (95.2 mg, 0.675 mmol), DMF (2 ml) and H_2O (0.5 ml) was prepared in a 20 ml scintillation vial and subsequently heated to 105 °C for 36 hours in a preheated oven. The as-synthesized sample was purified through repeated washing with DMF to yield small colourless rod-shaped crystals (Supplementary Fig. 9), which were stable and insoluble in common organic solvents (Supplementary Fig. 11). The crystals were harvested, soaked in DMF overnight and exchanged in MeOH for one week. MeOH was refreshed at least every 24 hours (Supplementary Figs 14, 16 and 33, and Supplementary Table 2).

Preparation of $[Cu_3(L){\cdot}(H_2O)_3]_n{\cdot}(solv)_x$, gea-MOF-2. A solution of Cu $(BF_4)_2{\cdot}2.5H_2O$ (1.8 mg, 0.0078 mmol), H_6L (1.6 mg, 0.0014 mmol), HNO_3 (3.5M,

0.1 ml), DMF (1.5 ml) and EtOH (0.5 ml) was prepared in a 20 ml scintillation vial and subsequently heated to 65 °C for seven days in a preheated oven. The as-synthesized sample was purified through repeated washing with DMF to yield small blue hexagonal-shaped crystals, which were insoluble in common organic solvents. The crystals were harvested, soaked in DMF overnight and then exchanged in EtOH for one week. EtOH was refreshed at least every 24 hours (Supplementary Figs 15, 17 and 34, and Supplementary Table 3).

Received 7 October 2013; accepted 16 May 2014; published online 29 June 2014

References

1. Eddaoudi, M. *et al.* Modular chemistry: secondary building units as a basis for the design of highly porous and robust metal–organic carboxylate frameworks. *Acc. Chem. Res.* **34,** 319–330 (2001).
2. Férey, G. Hybrid porous solids: past, present, future. *Chem. Soc. Rev.* **37,** 191–214 (2008).
3. Eubank, J. F. *et al.* The quest for modular nanocages: tbo-MOF as an archetype for mutual substitution, functionalization, and expansion of quadrangular pillar building blocks. *J. Am. Chem. Soc.* **133,** 14204–14207 (2011).
4. Eubank, J. F. *et al.* The next chapter in MOF pillaring strategies: trigonal heterofunctional ligands to access targeted high-connected three dimensional nets, isoreticular platforms. *J. Am. Chem. Soc.* **133,** 17532–17535 (2011).
5. Zhou, H. C., Long, J. R. & Yaghi, O. M. Metal–organic frameworks. *Chem. Rev.* **112,** 673–1268 (2012).
6. Long, J. R. & Yaghi, O. M. Metal–organic frameworks, *Chem. Soc. Rev.* **38,** 1201–1508 (2009).
7. Li, M., Li, D., O'Keeffe, M. & Yaghi, O. M. Topological analysis of metal–organic frameworks with polytopic linkers and/or multiple building units and the minimal transitivity principle. *Chem. Rev.* **114,** 1343–1370 (2014).
8. Eubank, J. F. *et al.* On demand: the singular rht net, an ideal blueprint for the construction of a metal–organic framework (MOF) platform. *Angew. Chem. Int. Ed.* **51,** 10099–10103 (2012).
9. Nouar, F. *et al.* Supermolecular building blocks (SBBs) for the design and synthesis of highly porous metal–organic frameworks. *J. Am. Chem. Soc.* **130,** 1833–1835 (2008).
10. O'Keeffe, M., Peskov, M. A., Ramsden, S. J. & Yaghi, O. M. The reticular chemistry structure resource (RCSR) database of, and symbols for, crystal nets. *Acc. Chem. Res.* **41,** 1782–1789 (2008).
11. Cavka, J. H. *et al.* A new zirconium inorganic building brick forming metal organic frameworks with exceptional stability. *J. Am. Chem. Soc.* **130,** 13850–13851 (2008).
12. Dan-Hardi, M. *et al.* A new photoactive crystalline highly porous titanium(IV) dicarboxylate. *J. Am. Chem. Soc.* **131,** 10857–10859 (2009).
13. Guillerm, V. *et al.* A zirconium methacrylate oxocluster as precursor for the low-temperature synthesis of porous zirconium(IV) dicarboxylates. *Chem. Commun.* **46,** 767–769 (2010).
14. Xue, D-X. *et al.* Tunable rare-earth fcu-MOFs: a platform for systematic enhancement of CO_2 adsorption energetics and uptake. *J. Am. Chem. Soc.* **135,** 7660–7667 (2013).
15. Guillerm, V. *et al.* A series of isoreticular, highly stable, porous zirconium oxide based metal–organic frameworks. *Angew. Chem. Int. Ed.* **51,** 9267–9271 (2012).
16. Morris, W. *et al.* Synthesis, structure, and metalation of two new highly porous zirconium metal–organic frameworks. *Inorg. Chem.* **51,** 6443–6445 (2012).
17. Du, D-Y. *et al.* An unprecedented (3,4,24)-connected heteropolyoxozincate organic framework as heterogeneous crystalline Lewis acid catalyst for biodiesel production. *Sci. Rep.* **3,** 2616 (2013).
18. Cairns, A. J. *et al.* Supermolecular building blocks (SBBs) and crystal design: 12-connected open frameworks based on a molecular cubohemioctahedron. *J. Am. Chem. Soc.* **130,** 1560–1561 (2008).
19. Alkordi, M. H. *et al.* Zeolite-like metal–organic frameworks (ZMOFs) based on the directed assembly of finite metal–organic cubes (MOCs). *J. Am. Chem. Soc.* **131,** 17753–17755 (2009).
20. Zheng, X-J., Jin, L-P. & Gao, S. Synthesis and characterization of two novel lanthanide coordination polymers with an open framework based on an unprecedented $[Ln_7(\mu\text{-}3\text{-}OH)_8]^{13+}$ cluster. *Inorg. Chem.* **43,** 1600–1602 (2004).
21. Devic, T., Serre, C., Audebrand, N., Marrot, J. & Férey, G. MIL-103, a 3-D lanthanide-based metal organic framework with large one-dimensional tunnels and a high surface area. *J. Am. Chem. Soc.* **127,** 12788–12789 (2005).
22. Park, Y. K. *et al.* Crystal structure and guest uptake of a mesoporous metal–organic framework containing cages of 3.9 and 4.7 nm in diameter. *Angew. Chem. Int. Ed.* **46,** 8230–8233 (2007).
23. Luo, J. *et al.* Hydrogen adsorption in a highly stable porous rare-earth metal–organic framework: sorption properties and neutron diffraction studies. *J. Am. Chem. Soc.* **130,** 9626–9627 (2008).
24. Lin, Z. *et al.* Pore size-controlled gases and alcohols separation within ultramicroporous homochiral lanthanide–organic frameworks. *J. Mater. Chem.* **22,** 7813–7818 (2012).
25. Lin, Z. *et al.* Ultrasensitive sorption behavior of isostructural lanthanide–organic frameworks induced by lanthanide contraction. *J. Mater. Chem.* **22,** 21076–21084 (2012).
26. Duan, J. *et al.* High CO_2/CH_4 and C_2 hydrocarbons/CH_4 selectivity in a chemically robust porous coordination polymer. *Adv. Funct. Mater.* **23,** 3525–3530 (2013).
27. Luebke, R. *et al.* The unique rht-MOF platform, ideal for pinpointing the functionalization and CO_2 adsorption relationship. *Chem. Commun.* **48,** 1455–1457 (2012).
28. Li, J-R. & Zhou, H-C. Metal–organic hendecahedra assembled from dinuclear paddlewheel nodes and mixtures of ditopic linkers with 120 and 90 degrees bend angles. *Angew. Chem. Int. Ed.* **48,** 8465–8468 (2009).
29. Suh, M. P., Park, H. J., Prasad, T. K. & Lim, D-W. Hydrogen storage in metal–organic frameworks. *Chem. Rev.* **112,** 782–835 (2012).
30. Sumida, K. *et al.* Carbon dioxide capture in metal–organic frameworks. *Chem. Rev.* **112,** 724–781 (2012).
31. Düren, T., Millange, F., Férey, G., Walton, K. S. & Snurr, R. Q. Calculating geometric surface areas as a characterization tool for metal–organic frameworks. *J. Phys. Chem. C* **111,** 15350–15356 (2007).
32. Koh, K., Wong-Foy, A. G. & Matzger, A. J. A porous coordination copolymer with over 5000 m^2/g BET surface area. *J. Am. Chem. Soc.* **131,** 4184–4184 (2009).
33. Wilmer, C. E. *et al.* Gram-scale, high-yield synthesis of a robust metal–organic framework for storing methane and other gases. *Energy Environ. Sci.* **6,** 1158–1163 (2013).
34. Yang, Q. *et al.* CH_4 storage and CO_2 capture in highly porous zirconium oxide based metal–organic frameworks. *Chem. Commun.* **48,** 9831–9833 (2012).
35. Guo, Z. *et al.* A metal–organic framework with optimized open metal sites and pore spaces for high methane storage at room temperature. *Angew. Chem. Int. Ed.* **50,** 3178–3181 (2011).
36. Peng, Y. *et al.* Methane storage in metal–organic frameworks: current records, surprise findings, and challenges. *J. Am. Chem. Soc.* **135,** 11887–11894 (2013).
37. Wu, H., Gong, Q., Olson, D. H. & Li, J. Commensurate adsorption of hydrocarbons and alcohols in microporous metal organic frameworks. *Chem. Rev.* **112,** 836–868 (2012).
38. Llewellyn, P. L. *et al.* Complex adsorption of short linear alkanes in the flexible metal–organic-framework MIL-53(Fe). *J. Am. Chem. Soc.* **131,** 13002–13008 (2009).
39. Bloch, E. D. *et al.* Hydrocarbon separations in a metal–organic framework with open iron(II) coordination sites. *Science* **335,** 1606–1610 (2012).
40. Klein, N., Henschel, A. & Kaskel, S. *n*-Butane adsorption on $Cu_3(btc)_2$ and MIL-101. *Micropor. Mesopor. Mater.* **129,** 238–242 (2010).
41. Omae, I. Recent developments in carbon dioxide utilization for the production of organic chemicals. *Coord. Chem. Rev.* **256,** 1384–1405 (2012).
42. Cokoja, M., Bruckmeier, C., Rieger, B., Herrmann, W. A. & Kühn, F. E. Transformation of carbon dioxide with homogeneous transition-metal catalysts: a molecular solution to a global challenge? *Angew. Chem. Int. Ed.* **50,** 8510–8537 (2011).
43. Roeser, J., Kailasam, K. & Thomas, A. Covalent triazine frameworks as heterogeneous catalysts for the synthesis of cyclic and linear carbonates from carbon dioxide and epoxides. *Chem. Sus. Chem.* **5,** 1793–1799 (2012).
44. Lescouet, T., Chizallet, C. & Farrusseng, D. The origin of the activity of amine-functionalized metal–organic frameworks in the catalytic synthesis of cyclic carbonates from epoxide and CO_2. *Chem. Cat. Chem.* **4,** 1725–1728 (2012).
45. Song, J. *et al.* MOF-5/*n*-Bu_4NBr: an efficient catalyst system for the synthesis of cyclic carbonates from epoxides and CO_2 under mild conditions. *Green Chem.* **11,** 1031–1036 (2009).
46. Monassier, A. *et al.* Synthesis of cyclic carbonates from epoxides and CO_2 under mild conditions using a simple, highly efficient niobium-based catalyst. *Chem. Cat. Chem.* **5,** 1321–1324 (2013).

Acknowledgements

Research reported in this publication was supported by the King Abdullah University of Science and Technology (KAUST).

Author contributions

V.G. and M.E. contributed to the conceptual approach to designing the material synthetic experiments; V.G. carried out the synthetic experiments; V.G., Ł.W. and K.A. conducted and interpreted the crystallographic experiments; V.G. performed the topological analysis; Y.B. and A.J.C. conducted and interpreted low- and high-pressure sorption experiments and IAST models (Y.B.); V.D. designed, conducted and interpreted catalysis experiments; V.G., M.E. and Ł.J.W. envisioned, designed and synthesized (Ł.J.W.) the organic hexacarboxylic ligand; V.G., Y.B. and M.E. wrote the manuscript.

Additional information

Supplementary information is available in the online version of the paper. Reprints and permissions information is available online at www.nature.com/reprints. Correspondence and requests for materials should be addressed to M.E.

Competing financial interests

The authors declare no competing financial interests.